Submitted to ApJL. Draft version dated March 30, 2016.
Preprint typeset using LaTeX style emulateapj v. 12/16/11

FRONTIER FIELDS CLUSTERS: THERMODYNAMICS OF THE LARGE-SCALE FILAMENT CROSSING MACS J0717.5+3745

G. A. Ogrean[1, †], R. J. van Weeren[2, ‡], C. Jones[2], T. Whalen[3], W. Forman[2]

[1]KIPAC, Stanford University, 452 Lomita Mall, Stanford, CA 94305, USA; gogrean@stanford.edu
[2]Harvard-Smithsonian Center for Astrophysics, 60 Garden Street, Cambridge, MA 02138, USA; and
[3]University of Maryland, College Park, MD 20742, USA;
Submitted to ApJL. Draft version dated March 30, 2016.

ABSTRACT
Keywords: Galaxies: clusters: individual: MACS J0717.5+3745 — Galaxies: clusters: intracluster medium — X-rays: galaxies: clusters

1. INTRODUCTION

In the ΛCDM cosmological model, structure in the universe is organized in a filamentary web in which large-scale cosmic filaments connect virialized massive structures such as clusters and groups of galaxies (e.g., Einasto et al. 1994). Approximately a third of the total bayonic matter is expected from hydrodynamic simulations to be contained in these large-scale filaments (e.g. Davé et al. 2001), in the form of low-density gas with temperatures of $10^5 - 10^7$ K. One of the main signatures of cosmic filaments is soft X-ray emission. However, the low density of the gas within the filaments poses a significant observational challenge, which causes detections to strongly depends on fortuitous alignments of the filaments with our line of sight. As a consequence, there have been only a handful of filament detections, among which the one in MACS J0717.5+3745 (Ebeling et al. 2004) and the one between A222-A223 (Dietrich et al. 2005; Werner et al. 2008).

Clusters of galaxies grow via the infall of gas and less massive structures along cosmic filaments (e.g., Springel et al. 2006). During infall and subsequent collision with the cluster, less massive structures will be ram-pressure stripped as they fly through the cluster's denser regions. Consequently, depending on their original density, these structures are either fully destroyed, or their compact cores survive and develop tails in their wake. An example of the latter scenario is seen in the cluster 1E 0657–558 (Elvis et al. 1992), in which the collision of a massive cluster with a cluster about 1/10 of its mass (Springel & Farrar 2007; Mastropietro & Burkert 2008) resulted in the famous "bullet" morphology of the less massive structure (Markevitch et al. 2002).

Here, we present results from *Chandra* observations of the merging galaxy cluster MACS J0717.5+3745. MACS J0717.5+3745 ($z = 0.546$; Ebeling et al. 2001, 2007) is one of the most complex merging systems discovered to date, being the site of collisions between four substructures (Ma et al. 2009; Medezinski et al. 2013). The superposition of the dark matter halos of these substructures also makes MACS J0717.5+3745 the largest known gravitational lens (Zitrin et al. 2009; Medezinski et al. 2013). The analysis of shallower *Chandra* observations of the cluster by Ma et al. (2009) found hot regions with temperatures $\sim$ 20 keV, remnant cool cores with temperatures of $\sim$ 5 keV, and density and temperature jumps at the interface between the cluster and the SE filament. The authors speculated that the jumps are caused accretion of gas from the filament onto the cluster. More recently, we have analyzed the thermodynamical properties of the ICM of MACS J0717.5+3745 using deeper *Chandra* observations (van Weeren et al., submitted). In this letter, we present the physical properties of the SE filament connected to MACS J0717.5+3745, and those of the substructures along the filament.

In Section 2, we summarize the processing of the *Chandra* datasets. The properties of the filament are discussed in Section 3, while those of the substructures in the filament are discussed in Section 4. The properties of the NW core that flew through the cluster are presented in Section 5. Our conclusions are summarized in Section **??**.

Throughout the paper we assume a ΛCDM cosmology with $H_0 = 70$ km s^{-1} Mpc^{-1}, $\Omega_{\rm m} = 0.3$, and $\Omega_\Lambda = 0.7$. For these parameters, 1 arcmin at the redshift of MACS J0717.5+3745 ($z = 0.546$) corresponds to a linear distance of approximately 383 kpc. Uncertainties on our measurements are quoted at the 90% level.

2. DATA PROCESSING AND BACKGROUND MODELING

Chandra observed MACS J0717.5+3745 four times between Jan 2001 and Dec 2013, for a total of 243 ks. Of the four ObsIDs, two (1655 and 16235) were taken in FAINT mode, while the other two (4200 and 16305) were taken in VFAINT mode. More details about the observation parameters can be found at the Chandra Data Archive.

The ObsIDs were reprocessed to apply the newest calibration files as of Jan 2004. Time periods affected by soft protons were removed from the data using the CIAO script *deflare*. The total clean exposure time after flare filtering was approximately 209 ks. Point sources were detected in the energy bands $0.5 - 2$ and $2 - 7$ keV using the script *wavdetect*, were visually confirmed, and excluded from the analysis. The instrumental background was subtracted using the stowed background files available in CalDB 4.6.3. Before subtraction, the instrumental background files were normalized to have the same $10 - 12$ keV count rate as the corresponding source files.

The sky background was modeled as the sum of unabsorbed emission from the Local Hot Bubble, absorbed emission from the Galactic Halo, and absorbed emission

† Hubble Fellow
‡ Clay Fellow

Table 1
Parameters of the regions used for the spectral analysis. The regions are shown in Figure 2. Uncertainties are quoted at the $\Delta C = 1$ level.

FOREGROUND AND BACKGROUND

Model Component	Temperature[a]	Normalization[b]
Local Hot Bubble	$0.135^{+0.007}_{-0.008}$	$7.21^{+0.30}_{-0.18} \times 10^{-7}$
Galactic Halo	$0.59^{+0.09}_{-0.08}$	$2.78^{+0.45}_{-0.44} \times 10^{-7}$
Unresolved Background Sources ObsID 16235/16305	–	$4.44^{+0.35}_{-0.37} \times 10^{-7}$
Unresolved Background Sources ObsID 4200	–	$7.02^{+0.49}_{-0.58} \times 10^{-7}$

LARGE-SCALE FILAMENT

Model Component	Temperature[a]	Normalization[b]
On Filament	$1.58^{+0.51}_{-0.25}$	$4.00^{+0.56}_{-0.60} \times 10^{-5}$
Off Filament	$11.55^{+9.09}_{-3.95}$	$1.55^{+0.14}_{-0.10} \times 10^{-5}$

GROUP IN THE FILAMENT

	Temperature[a]	Normalization[b]
	$3.87^{+0.66}_{-0.51}$	$(1.77 \pm 0.13) \times 10^{-4}$

FLY-THROUGH CORE

Model Component	Temperature[a]	Normalization[b]
Core	$6.82^{+1.88}_{-1.36}$	$3.41^{+0.29}_{-0.25} \times 10^{-4}$
N+S of Core	$7.47^{+1.11}_{-0.86}$	$2.08^{+0.77}_{-0.78} \times 10^{-4}$
Ahead of Core	$5.06^{+1.61}_{-0.98}$	$8.52^{+0.88}_{-0.77} \times 10^{-5}$
Behind Core	$10.89^{+2.05}_{-1.27}$	$3.92^{+0.10}_{-0.09} \times 10^{-4}$

[a] Units of keV.
[b] Units of cm^{-5} arcmin^{-2} for the thermal components, and photons keV^{-1} cm^{-2} s^{-1} arcmin^{-2} at 1 keV for the power-law components.

from unresolved X-ray sources. The hydrogen column density was fixed to 8.36×10^{20} cm^{-2}, corresponding to the sum of the atomic and molecular hydrogen column densities in the direction of MACS J0717.5+3745[4] (Kalberla et al. 2005; Willingale et al. 2013). All the foreground components were assumed to have solar metallicities equal to those reported by Feldman (1992).

A more detailed description of the data processing and the background modeling is provided by van Weeren et al., submitted. Our analysis can also be reproduced by the reader by downloading the datasets from the Chandra Data Archive and running the Jupyter notebook[5] available at `https://github.com/gogrean`.

3. LARGE-SCALE COSMIC FILAMENT

To define the region of the filament that is least contaminated by ICM emission, we examined the surface brightness profile in a rectangular region aligned with the filament. In this region, the surface brightness decreases away from the cluster center, and then increases again when the region intersects the SE group located along the filament; there is no radial range in this region where the surface brightness is flat. This suggests that the ICM of MACS J0717.5+3745 contaminates the filament, and this contamination needs to be considered when modeling the filament emission.

To model the filament and the contamination from the ICM, we extracted spectra in three rectangular regions: one centered on the filament, and two positioned to the W and to the E of it. These regions are shown in Figure 2. The regions were chosen to avoid the bright parts of the ICM, as well as emission from the SE galaxy group. The emission in the W and E regions was modeled with a single thermal component, while the emission in the filament region was modeled with two thermal components– one describing ICM contamination, whose parameters were linked to those of the thermal component used to describe the W and E regions, and one describing emission from the filament. The spectra from the three regions were fitted simultaneously. Table 1 lists the best-fitting parameters obtained for a gas metallicity of 0.2 solar. Varying the metallicity causes only minor changes to the best-fitting parameters, well within the statistical uncertainty ranges. In the JUPYTER notebook supporting this letter, we also show the results obtained for metallicities of 0 and 0.1 solar.

The XSPEC normalizations of the thermal components listed in Table 1 are defined as:

$$\mathcal{N} = \frac{n_\mathrm{e}\, n_\mathrm{H}\, V}{10^{14}\, \pi\, S_\mathrm{reg}\, D_\mathrm{A}^2\, (1+z)^2}\,,$$

if we assume the density to be constant in each region, where n_e is the electron number density, n_H is the hydrogen number density, V is the volume of the region, S_reg is the projected area of the region, D_A is the angular size distance to the cluster, and z is the cluster redshift.

To calculate the density of the filament in the region shown in Figure 2, we assumed this region has an elliptic cylinder geometry. Jauzac et al. (2012) determined that the filament is inclined at 75 degrees with respect to the plane of the sky, and has a diameter of ~ 1.6 Mpc and a length of ~ 19 Mpc. Therefore, we assumed the region from which we extracted the spectrum of the filament to be an elliptic cylinder with a length:

$$L = \frac{l_\mathrm{box}}{\cos 75^\circ} \sim 2.2 \text{ Mpc} \qquad (1)$$

where l_box is the length of the box region in Figure 2, and a base with major axis $a = 0.8$ Mpc and a minor axis equal to the length of the box in Figure 2, i.e. $b = 0.2$ Mpc. The volume of this region is $V = \pi a\, b\, L = 1.1$ Mpc^3. We further assumed that $n_\mathrm{H} = 1.2\, n_\mathrm{e}$ (Böhringer & Werner 2010). The area of the filament region shown in Figure 2 is 1.4 arcmin^2. Therefore, for an XSPEC normalization of $\sim 4 \times 10^{-5}$ cm^{-5} arcmin^{-2} (Table 1), the electron number density is $\sim 1 \times 10^{-4}$ cm^{-3}. Assuming a baryon fraction of 0.044 (Kirkman et al. 2003), the filament is over-dense by a factor of ~ 250 compared to the mean baryon density of the Universe. Our result is consistent with that of Jauzac et al. (2012), who used lensing data to calculate a filament over-density factor of 206 ± 46.

For a baryon fraction of 0.15 (Mantz et al. 2014), the density of the filament is equivalent to a mass of $\sim 2 \times 10^{13}$ M$_\odot$ Mpc^{-3}. Approximating the geometry of the full filament as a cylinder with a length of 19 Mpc and a diameter of 1.6 Mpc, our result implies a total filament mass of $\sim 7 \times 10^{14}$ M$_\odot$.

4. GROUP IN THE FILAMENT

[4] http://www.swift.ac.uk/analysis/nhtot/index.php
[5] Running the notebook requires the bash_kernel package.

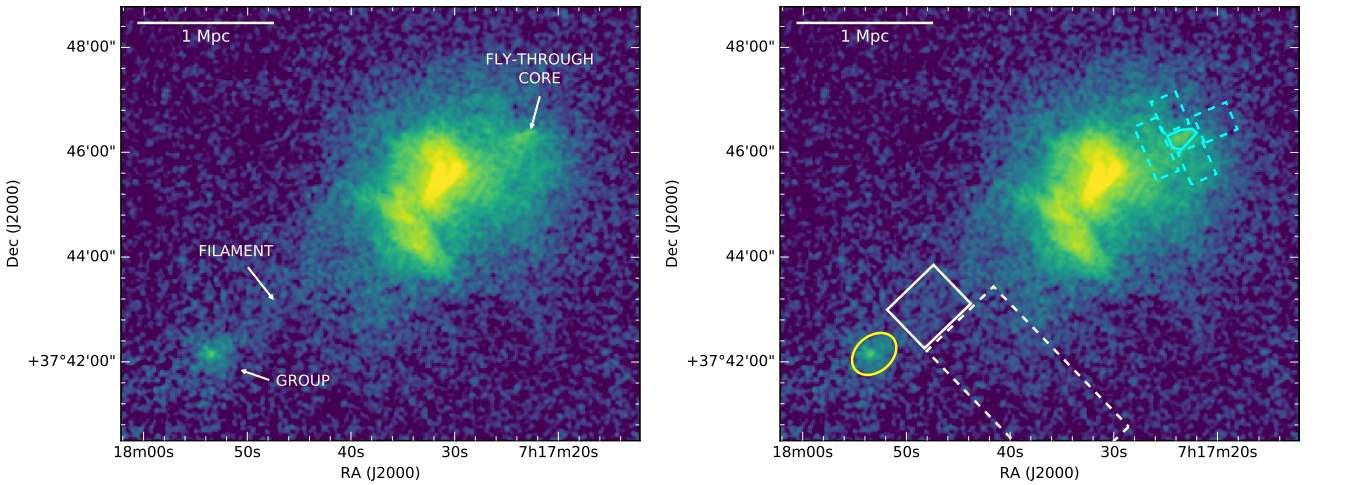

Figure 1. *Left:* Chandra $0.5-4$ keV surface brightness map of MACS J0717.5+3745, showing the features discussed in this work. The image was exposure- and vignetting-corrected. Point sources were subtracted and the gaps were filled by sampling the regions surrounding the point sources.[a] *Right:* Regions used in the spectral analysis. The regions of main interest are drawn in solid lines, while the regions used to characterize the contaminating/surrounding emission are drawn in dashed lines. The best-fitting parameters obtained for the gas in these regions are listed in Table 1.

[a]The gaps were filled to create a more visually appealing figure. However, the imaging analysis was done on images that did not have the gaps filled. The images used in the analysis are available online as supporting material.

The group of galaxies within the large-scale filament is located a little over 2 Mpc SE of the cluster center, chosen to be at RA = 07 : 17 : 30.025, Dec = +37 : 45 : 18.58. The small size of the group and its large distance from the cluster implies that it is falling for the first time towards MACS J0717.5+3745, rather than having traversed the cluster from the NW to the SE.

We measured the temperature and the brightness of the cluster by extracting spectra from an elliptical region shown in Figure 2. We assumed a group metallicity of 0.2 solar. The best-fitting parameters are summarized in Table 1. The normalization is equivalent to a luminosity of $(1.05 \pm 0.09) \times 10^{43}$ erg s^{-1}. Based on the luminosity-mass scaling relations for galaxy groups (e.g., Connor et al. 2014), the group's luminosity corresponds to a mass of $\sim 5 \times 10^{13}$ M$_{\odot}$.

5. FLY-THROUGH CORE

Approximately 670 kpc NW of the cluster center, there is a bright X-ray core with a tail extending $\sim$ 200 kpc towards SE, roughly in the direction of the large-scale filament discussed in Section 3. This morphology suggests that this core, seen 'flying' through the ICM of MACS J0717.5+3745 and ram-pressured stripped by the cluster's dense ICM, traveled NW along the SE filament and is seen after it traversed the brightest ICM regions. In essence, the core is a later stage of the group currently seen within the filament.

The core is still embedded (at least in projection) in the ICM of MACS J0717.5+3745. To determine the core's physical properties, we modeled the contamination from the ICM by extracting spectra N and S of the core. These spectra were modeled with a thermal component with a metallicity of 0.2 solar. We assumed the spectral properties were the same in the N and S regions. The spectra of the core were modeled as the sum of emission from the contaminating ICM and from the core itself. The spectra of the core and of the regions N and S of it were modeled in parallel. The best-fitting results are summarized in Table 1. The temperature of the core, $6.82^{+1.88}_{-1.36}$ keV, is consistent with the temperatures N and S of the core, in regions that are approximately at the same distance from the cluster center as the core. We also compared the core temperature with the temperatures ahead of (NW) and behind (SE) the core. The temperature decreases from $10.89^{+2.05}_{-1.27}$ keV behind the core, to $5.06^{+1.61}_{-0.98}$ keV ahead of the core. From these temperature measurements, we therefore find no evidence of a particularly cold core or of a temperature discontinuity (either a shock or a cold front) ahead of the core.

A cold front and a shock front would be expected ahead of the core, similarly to the features seen in the Bullet Cluster (Markevitch et al. 2002) and in front of the group NGC 4839 infalling into the Coma Cluster (Neumann et al. 2001) ***other citation needed here for the cold front***. We searched for possible evidence of a cold/shock front by fitting the surface brightness profile of the group with a broken power-law density model. However, our imaging analysis did not reveal a density discontinuity significant at the 1σ confidence level. Nevertheless, we cannot exclude the existence of a density discontinuity in front of the core. The small size of the core and the additional substructure in the ICM make the modeling difficult despite *Chandra*'s high spatial resolution. Furthermore, the core could be moving in a direction away from the plane of the sky, which would make the detection of a density discontinuity even more challenging; indeed, if the core originated from the large-scale filament, its movement is unlikely to be in the plane of the sky.

REFERENCES

Böhringer, H., & Werner, N. 2010, A&A Rev., 18, 127
Connor, T., Donahue, M., Sun, M., et al. 2014, ApJ, 794, 48
Davé, R., Cen, R., Ostriker, J. P., et al. 2001, ApJ, 552, 473
Dietrich, J. P., Schneider, P., Clowe, D., Romano-Díaz, E., & Kerp, J. 2005, A&A, 440, 453
Ebeling, H., Barrett, E., & Donovan, D. 2004, ApJ, 609, L49
Ebeling, H., Barrett, E., Donovan, D., et al. 2007, ApJ, 661, L33
Ebeling, H., Edge, A. C., & Henry, J. P. 2001, ApJ, 553, 668

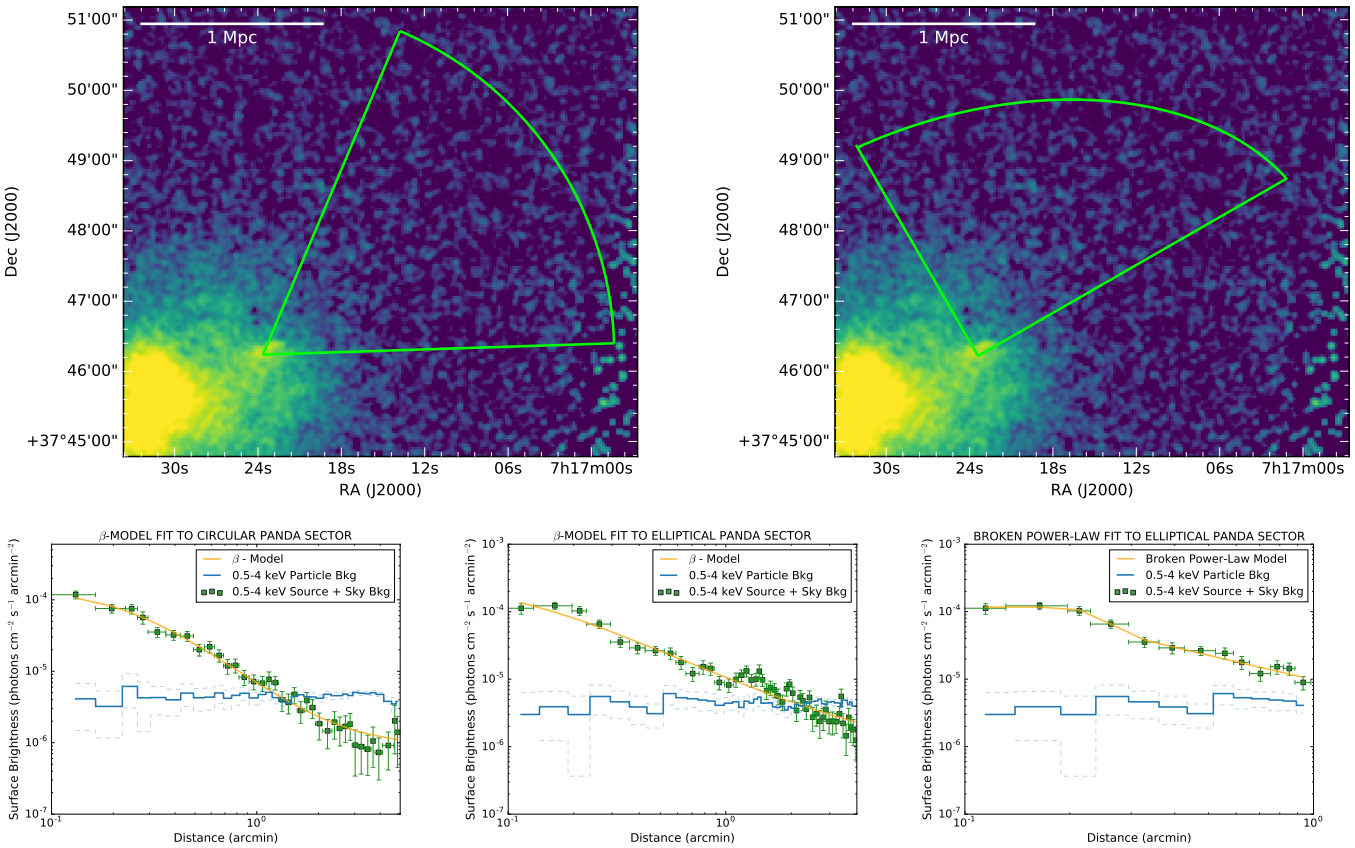

Figure 2. *Left:* Chandra $0.5-4$ keV surface brightness map of MACS J0717.5+3745, showing the features discussed in this work. The image was exposure- and vignetting-corrected. Point sources were subtracted and the gaps were filled by sampling the regions surrounding the point sources.[a] *Right:* Regions used in the spectral analysis. The regions of main interest are drawn in solid lines, while the regions used to characterize the contaminating/surrounding emission are drawn in dashed lines. The best-fitting parameters obtained for the gas in these regions are listed in Table 1.

[a]The gaps were filled to create a more visually appealing figure. However, the imaging analysis was done on images that did not have the gaps filled. The images used in the analysis are available online as supporting material.

Einasto, M., Einasto, J., Tago, E., Dalton, G. B., & Andernach, H. 1994, MNRAS, 269, 301
Elvis, M., Plummer, D., Schachter, J., & Fabbiano, G. 1992, ApJS, 80, 257
Feldman, U. 1992, Phys. Scr, 46, 202
Jauzac, M., Jullo, E., Kneib, J.-P., et al. 2012, MNRAS, 426, 3369
Kalberla, P. M. W., Burton, W. B., Hartmann, D., et al. 2005, A&A, 440, 775
Kirkman, D., Tytler, D., Suzuki, N., O'Meara, J. M., & Lubin, D. 2003, ApJS, 149, 1
Ma, C.-J., Ebeling, H., & Barrett, E. 2009, ApJ, 693, L56
Mantz, A. B., Allen, S. W., Morris, R. G., et al. 2014, MNRAS, 440, 2077
Markevitch, M., Gonzalez, A. H., David, L., et al. 2002, ApJ, 567, L27
Mastropietro, C., & Burkert, A. 2008, MNRAS, 389, 967
Medezinski, E., Umetsu, K., Nonino, M., et al. 2013, ApJ, 777, 43
Neumann, D. M., Arnaud, M., Gastaud, R., et al. 2001, A&A, 365, L74
Springel, V., & Farrar, G. R. 2007, MNRAS, 380, 911
Springel, V., Frenk, C. S., & White, S. D. M. 2006, Nature, 440, 1137
Werner, N., Finoguenov, A., Kaastra, J. S., et al. 2008, A&A, 482, L29
Willingale, R., Starling, R. L. C., Beardmore, A. P., Tanvir, N. R., & O'Brien, P. T. 2013, MNRAS, 431, 394
Zitrin, A., Broadhurst, T., Rephaeli, Y., & Sadeh, S. 2009, ApJ, 707, L102